Kinetics of Reduction of Nickel Oxide with CO

J. H. KRASUK and J. M. SMITH

Department of Chemical Engineering
University of California, Davis, California 95616

Initial rates were measured for the reduction of single pellets of nickel oxide with carbon monoxide at atmospheric pressure and temperatures from 566 to 796°C. The nickel oxide pellets were porous ($\bar{\epsilon}_0 = 0.032 - 0.35$) and intrapellet diffusion retarded the rate so that the shrinking core model was not applicable. Effective diffusivities for the lower porosity pellets were very small, corresponding to tortuosity factors of about 180 for $\bar{\epsilon}_0 = 0.032$ and 92 for $\bar{\epsilon}_0 = 0.062$.

The reaction appeared to be first order in carbon monoxide. Rate constants, based upon the intraparticle area, indicated an activation energy of 47 kcal/g.-mole over the temperature range 566 to 682°C. At higher temperatures the rate was constant. These results, while not conclusive, are in agreement with a reaction sequence consisting of formation of nuclei of nickel atoms in the nickel oxide surface, rapid adsorption of carbon monoxide at the nickel-nickel oxide interface, migration of the adsorbed carbon monoxide to the adjacent lattice, and a slow reaction to extract oxygen from the lattice.

The reduction of ores is a major industry throughout the world, yet the design of reduction equipment has not advanced to the level of many other kinds of reaction apparatus, for example, fixed-bed catalytic reactors. An appropriate starting point for improving design concepts is a study of the intrinsic kinetics of the gas-solid, noncatalytic reactions that occur during reduction. Metallic oxides are seldom nonporous. Hence, observed rates are not a measure of intrinsic kinetics due to coupling with transport processes and by uncertainty about the true reaction area. To avoid these problems data have heretofore been analyzed (*3, 10, 12, 17*) by the shrinking-core model (*19*). Except for those few cases where a very sharp boundary exists between unreacted oxide and metal product, this model gives unrealistic rate constants and activation energies. The present work was undertaken in order to obtain realistic rate constants (intrinsic kinetics) by measuring intraparticle areas and accounting for intraparticle diffusion for a practical system.

Intrinsic kinetics were investigated for the reduction of nickel oxide pellets with carbon monoxide in the presence of carbon dioxide. Initial rates were measured gravimetrically for single, sintered pellets with porosities of 0.35 to 0.032. Pore-volume distributions were used to evaluate reaction areas and, with the rate data, to obtain effective diffusivities for the pellets of lower porosity.

The reduction reaction

$$CO(g) + NiO(s) \rightarrow CO_2(g) + Ni(s)$$

is essentially irreversible up to temperatures above 796°C. Also the operating conditions were chosen (temperatures of 566 to 796°C. and carbon monoxide partial pressures of 0.07 to 0.33 atm.) such that no deposition of carbon by the reaction $2CO \rightarrow C + CO_2$ was predicted from thermodynamic information. X-Ray analysis of some of the pellets after reduction verified the absence of carbon and of Ni_3C. Both substances might be produced at lower temperatures and higher carbon monoxide concentrations. The system had other advantages: equimolar counter diffusion of carbon monoxide and carbon dioxide, a single solid product, and low heat of reduction ($\Delta H = -10{,}150$ cal/g.-mole) so that intrapellet temperature gradient were negligible.

Correspondence concerning this paper should be addressed to J. M. Smith. J. H. Krasuk is with the University of Chile, Santiago, Chile.

EXPERIMENTAL STUDIES

Apparatus

The apparatus for the kinetic studies is shown in Figure 1. The weight of the pellet in the stirred-tank, monel reactor could be measured at short time intervals during the course of the reaction. The reactor was originally developed to study the hydro-fluorination of uranium dioxide, and dimension and construction details have been published (*3*). Two preheaters, one an integral part of the reactor, were used to achieve a constant temperature of the carbon monoxide-carbon dioxide feed. In all runs the temperature determined by an iron-constantan thermocouple (located in the gas space above the pellet) was recorded. For selected runs, temperatures within the pellet were also measured. The wire connecting the pellet and the Mettler H3 balance (sensitivity = 1 mg.) extended through a vertical chamber and was maintained in alignment by pinholes at the top and bottom of the chamber. A small flow of carbon dioxide monitored by valve V3 (Figure 1) was introduced to the vertical chamber in order to prevent introduction of air via the pinholes.

Pellet Manufacture and Porosity

The pellets were made by pressing and sintering nickelous oxide (J. T. Baker Company., 99.6% NiO). The powderous material had been produced by hammer milling and passed through 325 mesh screen (particle size less than 44 microns). Its surface area was 3-5 sq. m./g. Without lubricant or

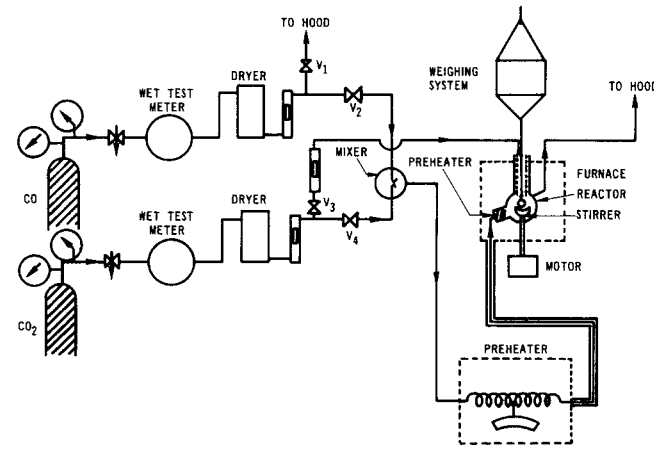

Fig. 1. Apparatus.

binder, hemispherical pellets of 2 cm diam. were prepared by applying 20,000 lb./sq.in.abs. pressure in a laboratory press. Thin polyethylene hemispherical caps, fitting into the die, prevented adherence of pellets to the die.

Pellets of successively lower porosity were prepared by varying the sintering process. The first stage consisted of heating the hemispheres for 46 hr. at 1150°C., with 4-hr. periods for heating and cooling. This treatment produced pellets of about 35% porosity ($\bar{\epsilon}_0 = 0.35$) with a diameter of about 1.7 cm. Such pellets were used for the runs at high porosity. Intermediate porosity ($\bar{\epsilon}_0 = 0.062$, diam. = 1.64 cm) pellets were produced by an additional sintering treatment of 7 hr. at 1650°C., also with 4-hr. heating and cooling periods. The lowest porosity ($\bar{\epsilon}_0 = 0.032$) was obtained by resintering the sinters from the first stage at 1765°C. for 15 hr., with heating and cooling periods of 3 hr. each. The diameter at this stage was about 1.40 cm.

It was necessary to feed air to the furnace when sintering at 1650° and 1765°C. in order to prevent formation of nickel. The reduction in diameter was due in part to vaporization of nickel oxide. Color changes occurred during sintering from yellow green (1150°C.) to dark green (1765°C.). Because of deformation of the die used to press the nickel oxide powder, similar sintering and pelleting conditions did not necessarily mean identical porosities. For example, immediately after remaking the die to ensure spherical geometry, the lowest porosity level was obtained after the first stage of sintering (pellet #57, Table 1).

The density of the nickel oxide powder was determined in a Beckman air pycnometer to be 6.75 g./cm^3. This agrees well with the solid density of nickel oxide, indicating that the particles contained no completely enclosed pores. However, the sintered pellets contained both closed and open pores so that it was desirable to measure two porosities. The apparent density ρ_a was determined from the pellet mass and total volume, as measured in the pycnometer by closing the open pores with paraffin. Substituting ρ_a for the density in the equation

$$\epsilon = 1 - \frac{\rho}{6.75} \tag{1}$$

gave the total porosity ϵ_T. The density ρ_s of the pellet when the open pores were not filled with paraffin was determined in a similar way. Substitution of ρ_s into Equation (1) gave the porosity ϵ_s of the closed pores. The open porosities were then obtained by difference; that is,

$$\epsilon_0 = \epsilon_T - \epsilon_s \tag{2}$$

Differences in ϵ_0 could be large for duplicate pellets of the lowest porosity ($\bar{\epsilon}_0 = 0.032$) but were but 2 to 3% when $\bar{\epsilon}_0 = 0.35$. Duplicate measurements were made for each pellet. The individual values of ϵ_T and ϵ_0 at each porosity level ($\bar{\epsilon}_0$) are given in Table 1.

The open porosity for completely reduced pellets was found to be 0.2 to 0.3.

Pore Size Distribution and Surface Area

Figure 2 illustrates the pore-volume distribution for a high porosity pellet, as determined in a mercury porosimeter. The maximum pressure of the instrument was 5000 lb./sq.in.abs., which corresponded to an equivalent circular pore of 350Å (0.035 microns) diameter. The distribution is also shown for the nickel product ($\epsilon_0 = 0.29$) which was obtained by completely reducing a nickel oxide pellet for which $\epsilon_0 = 0.34$. Since the curves are flat between 0.2 and 0.06 microns, there appear to be no pores smaller than 350Å. Since the pellets had to be broken before measuring the pore volume, the pellets of nickel oxide used for reaction runs could not be em-

Table 1. Estimation of Kinetic Constants from Initial Rates of Reaction ($p_t = 1$ atm.)

Pellet no.	Run no.	Porosity level $\bar{\epsilon}_0$	Total porosity ϵ_T	Open porosity ϵ_0	Apparent density ρ_a g cm^3	Pellet volume V, cm^3	Pellet external Area S_{ex} cm^2	Initial mass of sample M_0 g	Specific surface area $\overline{S_g}$ sq.m/g	Average pore diameter $\overline{\delta} \times 10^4$ cm
19	5		0.105	0.070	6.044	2.530	8.89	15.29		
10	6		0.118	0.058	5.955	2.527	8.95	15.05		
16	11		0.089	0.076	6.151	2.430	8.76	14.94		
20	9	0.062	0.124	0.050	5.913	2.48	8.93	14.66	0.133	0.338
8	19		0.118	0.080	5.958	2.37	8.64	14.12		
27	20		0.131	0.087	5.869	2.40	8.67	14.08		
24	21		0.09	0.060	6.101	2.45	8.79	14.97		
12	23		0.116	0.093	5.966	2.49	8.87	14.85		
67	27		0.043	0.018	6.461	0.754	4.605	4.87		
36	28		0.069	0.020	6.289	1.032	5.695	6.49		
40	36	0.032	0.084	0.030	6.188	1.136	6.329	7.02	0.0667	0.432
57	68		0.12	0.010	5.948	1.037	5.885	6.16		
33	39		0.10	0.036	6.065	1.379	6.25	8.36		
45	62		0.334	0.334	4.573	2.297	8.762	10.50		
74	63	0.35	0.345	0.345	4.455	2.690	9.635	11.98	0.564	0.521
28	65		0.374	0.374	4.276	2.237	8.413	9.56		
22	64		0.359	0.342	4.326	2.823	9.853	12.21		
90	42		0.0581	0.0418	6.360	0.933	5.701	5.93		
80	43		0.0594	0.0241	6.351	1.08	5.861	6.85		
60	44		0.0645	0.0291	6.317	0.755	4.679	4.77		
65	45		0.104	0.051	6.050	1.215	6.433	7.35		
54	48	0.032	0.093	0.045	6.121	0.683	4.549	4.18	0.0667	0.432
49	49		0.113	0.027	5.986	0.645	4.166	3.86		
46	54		0.100	0.040	6.05	0.744	4.43	4.50		
89	55		0.131	0.010	5.869	0.692	4.197	4.06		
82	59		0.071	0.049	5.798	0.800	4.635	4.64		
22	64	Ni Product	0.29	0.29					0.185	0.860

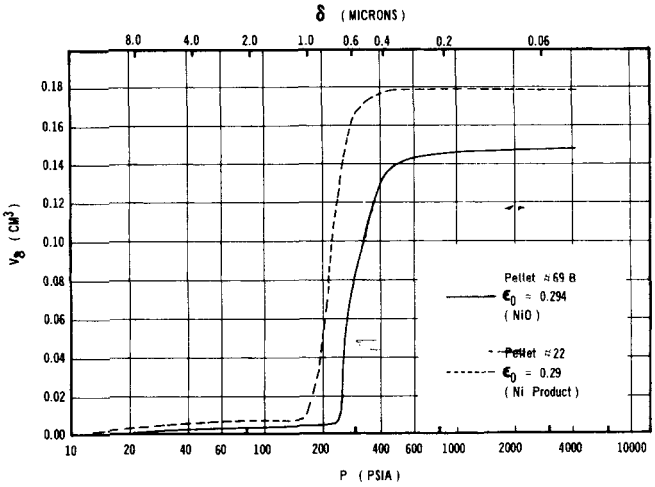

Fig. 2. Pore-volume distribution for high-porosity pellet and reacted product.

ployed for pore-volume studies. Two pellets at each porosity level were prepared for the pore-volume measurements.

The surface area S_g was evaluated by assuming that the pores were cylindrical and using the pore-volume distribution to determine the product, $n_i L_i$, of the length and number of pores of diameter δ_i. The resulting equation for S_g is

$$S_g = \frac{4}{M_0}\int_0^\infty \frac{D(\delta)}{\delta}\,d\delta \qquad (3)$$

where the pore-volume distribution function is

$$D(\delta) = \frac{dV_\delta}{d\delta} \qquad (4)$$

$D(\delta)$ is obtained by differentiating curves of the type shown in Figure 2. This method of evaluating S_g does not require any suppositions about the mean-pore diameter $\overline{\delta}$. A number for $\overline{\delta}$ can be obtained by assuming a model for the pore system. If, as is often done in catalyst pellets, the volume and surface of the pores are assumed to be given by a system of n parallel pores of diameter $\overline{\delta}$ and length $\overline{L}$, then

$$\overline{\delta} = \frac{V_{\epsilon_0}}{\int_0^\infty \frac{D(\delta)}{\delta}\,d\delta} \qquad (5)$$

The values for $\overline{S_g}$ and $\overline{\delta}$ for the two sets of data at each porosity level were averaged, and the results are given in last two columns of Table 1. The area of the nickel oxide pellets decreased about 8-fold between the highest and lowest porosity. It will be noted later that the reaction rate decreased much more. Since the pellet (#22) of nickel product originated from a high porosity nickel oxide, it can be concluded that the reaction process was accompanied by a large (3-fold) decrease in surface area. This is due to the intense sintering which accompanied reaction in the high-porosity pellets. For example, the initial volume of pellet #22 was 2.82 cm³, and after complete reduction at 767°C, its volume was 1.28 cm³. It was possible to achieve complete reduction only for the pellets of highest porosity. For other porosities conversions were low even after 2½ hr.

Operating Procedures

Since pellet temperatures could not be measured without disrupting the weighing procedure, separate runs were made with thermocouples placed at the center and surface of the pellet. For the center temperature, a groove was made in the circular faces of two hemispheres. A 24 gauge iron-constantan thermocouple was placed at the midpoint of the groove, and the two hemispheres were sealed into a spherical pellet with Insalute #1 cement. Surface temperatures were measured by placing the thermocouple at a location in the groove near the outer surface. The temperature runs were made at the same conditions (flow rates and gas thermocouple reading) as used for the reaction runs.

For the reactions runs at intermediate and high porosity, two hemispheres were cemented together to form a spherical pellet. Observation of the color of partially reacted pellets indicated that the cement provided an impermeable barrier for carbon monoxide. Hemispheres were employed for the low porosity runs.

Geometric measurements were made on the pellets with a micrometer in order to evaluate the external surface. The pellet volumes calculated from these measurements agreed within 2% of the total volume (with paraffin to close the pores) determined in the pycnometer.

Before the initiation of a run, it was necessary to align the weight-measuring system so that the observed weight, with the stirrer operating, agreed with the predetermined weight of the pellet, holder, and wire. With proper precautions smooth curves of weight versus time were possible for the two higher porosity levels. At the lowest porosity, the maximum weight change was so low (< 30 mg) that weighing uncertainties were significant. These uncertainties were caused by vibrations due to the stirrer and amounted to $\pm$ 2 mg. The data in Figure 3, showing typical results, illustrate the situation. However, an accurate value for the final weight of the low porosity pellet could be obtained at the end of the run by removing it from the equipment. Since the conversion was so small ($< 4.7\%$) for the lowest porosity pellets, the rate did not change appreciably during the run. Hence, the values of the initial and final weights were sufficient to obtain a reasonable value for the initial rate.

PRELIMINARY OBSERVATIONS

X-Ray diffraction studies were made of the flat, circular surfaces of reacted and original nickel oxide pellets. The patterns obtained were compared with standards for Ni_3C, Ni_xC, NiO, Ni, C. The completely reacted pellets showed very intense patterns corresponding to nickel and only weak patterns of nickel oxide. These pellets had been exposed to carbon monoxide for reaction times of 1.5 hours, after which there was no further, detectable change in weight. This suggests that the small residual nickel oxide reacted very slowly. The observed weight change during reaction for these pellets agreed within experimental error with that expected stoichiometrically for complete conversion. In the lowest-porosity pellets the conversion was always low, and these pellets showed patterns for both nickel oxide and nickel. In all cases no other components than nickel oxide and nickel were identified. A gravimetric analysis employing dimethyl glyoxime (7) was carried out on one of the pellets sintered at 1650°C. ($\bar{\epsilon}_0 = 0.062$). The result gave 99.3% nickel oxide in comparison with 99.6% stated by the manufacturer.

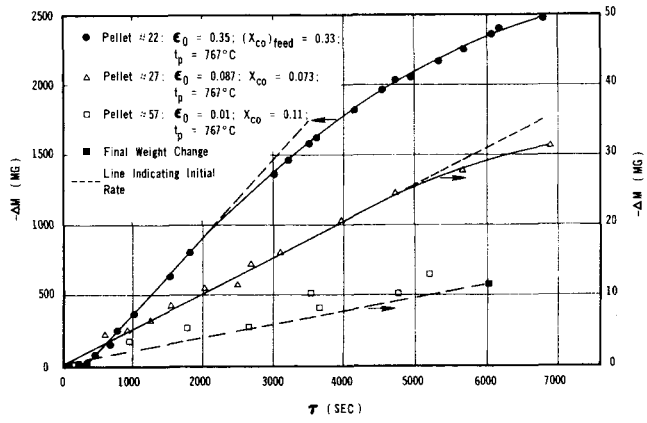

Fig. 3. Typical weight-loss runs for different porosities.

TEMPERATURE AND CONCENTRATION DIFFERENCES

At the temperature levels employed, radiation between pellet and reactor wall was important. Therefore, the temperature t_g measured by the thermocouple in the gas phase, which was itself subject to radiation errors, was not equivalent to the pellet temperature t_p. The gas-phase thermocouple read as much as 83°C. less than pellet-surface termocouples.

In the runs where both surface and center temperatures were measured, the maximum difference was 2°C. Hence intraparticle temperature gradients were neglected, and it was assumed that the reaction occurred at the temperature measured at the center of the pellet.

The rate of heat evaluation due to reaction was so low for the lowest porosity pellets that the temperature did not change with time. This is illustrated by the temperature traces for pellet #56 ($\bar{\epsilon}_0 = 0.032$) in Figure 4. However, for the highest porosity pellets the temperature rose significantly. The absolute levels in Figure 4 are also affected by flow rates and preheater settings.

Concentration differences for carbon monoxide between bulk gas and pellet surface were estimated by evaluating mass transfer coefficients from correlations (*1, 11*) for systems as similar to that in Figure 1 as possible. The stirrer speed was set at a high value, 1,720 rev./min. to provide stirred-tank operation. This approach indicated that for the highest reaction rate the fractional change in concentration was less than 2%. Hence, the surface concentration was taken equal to the value in the outlet stream from the reactor. High flow rates (about 1 liter/min. at 28°C. and 1 atm.) of CO + CO_2 were used to minimize changes in gas composition due to reaction. For the lowest and intermediate porosity levels, these flow rates were large enough that the exit composition was not significantly different from that of the feed. For the high rates of reaction corresponding to the highest porosity level, the two compositions differed as much as 13%. For these cases $(X_{CO})_{exit}$ was evaluated from the known feed composition by the equation

$$(X_{CO})_{exit} = (X_{CO})_{feed} - \left(-\frac{dn}{d\tau}\right)\frac{1}{F} \qquad (6)$$

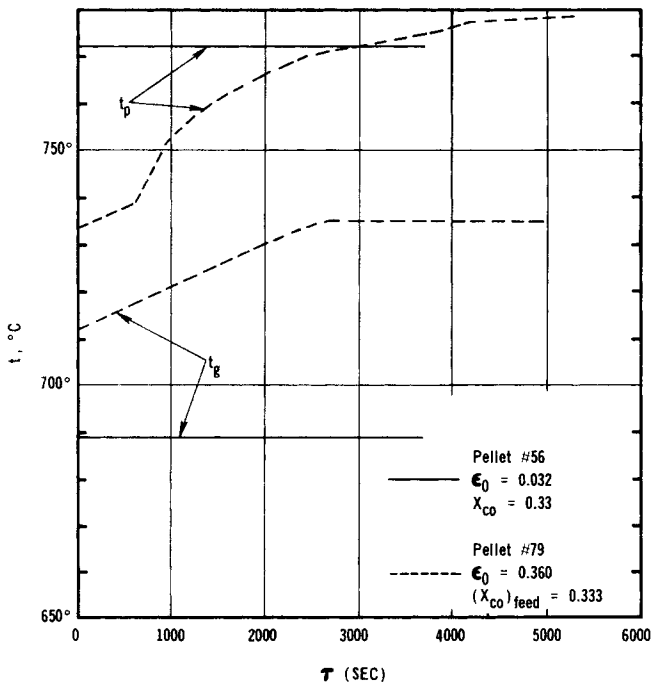

Fig. 4. Pellet (center) and gas thermocouple temperatures.

Here $-dn/d\tau$ is the rate of reaction obtained from the weight versus time measurements, as described in the next section.

VISUAL OBSERVATIONS

Examination of partially reacted pellets indicated that intrapellet concentration gradients existed in the nickel oxide. For example, when pellets for which $\bar{\epsilon}_0 = 0.062$ were broken, a grey, outer shell could be observed. The central core was green, corresponding to nickel oxide. The thickness of the grey shell corresponded to a conversion of about 70%, assuming that the material was entirely nickel. However, the weight change gave a conversion of but 7%. After complete reduction, which was possible for the high porosity pellets, broken pellets had a uniform, silvery color. A similar discrepancy existed between the actual conversion and the thickness of the grey layer for partially reacted pellets of other porosities. It was concluded that the outer layer was but partially reduced and that reaction and diffusion occurred simultaneously within this region of nickel oxide plus nickel. Accordingly, the rate data were analyzed in terms of an intrinsic rate combined with an effectiveness factor.

INITIAL RATE RESULTS

At zero time the rate of reaction was not influenced by the presence of the reaction product, for example, by diffusion resistances through regions of nickel. As Figure 3 indicates, the reaction was slow enough that the rate of change of mass was constant over a significant time interval, more than 1,000 sec. for the most rapid rate (highest porosity). Hence, the slope of the lines as $\tau \to 0$ in plots such as Figure 3 were used to calculate the molal rate of reaction $(-dn/d\tau)_0$ per pellet. As already mentioned, for the lowest-porosity pellet the weight loss was established from measurement of the pellet weight at the end of the run. For the highest-porosity pellets there was an induction period of a few minutes before the rate assumed its normal value. This is illustrated by the data for pellet #22 in Figure 3, and is believed to be due to the necessity to form nickel oxide-nickel interfaces before reaction can proceed.

The temperatures, gas compositions, and rates for all the runs are given in Table 2. The rates per pellet increase more than 100 times as $\bar{\epsilon}_0$ increased from 0.032 to 0.35. The corresponding increase in surface area $\bar{S}_g M_0$ is of the order of 15 times. This difference indicates that either the intrinsic rate decreases as the porosity is decreased, corresponding to increased sintering, or that significant diffusion resistances exist in the nickel oxide pellets. The effect of sintering on intrinsic activity was tested by preparing low-porosity pellet (#57) with only the first, mild (1150°C.) sintering stage. This was possible by remaking a worn die to conform more closely to exact hemispherical geometry. Using this die, the unsintered pellet was much more compact, and mild sintering was sufficient to reduce ϵ_0 to a low value. The rate per unit area Ω for pellet #57 agrees well (Figure 5) with the data for the other pellets in the $\bar{\epsilon}_0 = 0.032$ group. These other pellets were prepared by severe sintering (1765°C.). In view of this result, and the visual observations, it is concluded that diffusion resistances in nickel oxide do exist and that it is appropriate to interpret the rate data accordingly.

EVALUATION OF KINETIC CONSTANTS

To eliminate area effects, specific rates Ω were obtained by dividing $(-dn/d\tau)_0$ by $M_0\bar{S}_g$. These rates at 767°C.

are plotted versus X_{CO} in Figure 5. Lines with slope of unity fit the data reasonably well. When the rates of a first order reaction are evaluated at constant pressure, as in the present system, the reaction order is not modified by intrapellet diffusional effects. Hence, the data in Figure 5 suggest that the reaction may be treated as first order. The higher Ω values for the high porosity pellets are expected, in view of diffusion effects. However, the data for the lowest porosity would be expected to fall below the line for $\bar{\epsilon}_0 = 0.062$. Instead it is slightly above. Part of the explanation may be that the mean pore diameter is greater for the lowest-porosity pellets (see $\overline{\delta}$ values in Table 1). However, as already mentioned, $\overline{S}_g$ and ϵ_0 values are subject to large errors when $\epsilon_0 \to 0$, and so the data points of the line for $\bar{\epsilon}_0 = 0.032$ in Figure 5 are somewhat uncertain.

In terms of the effectiveness factor η the rate equation may be written

$$\Omega = \eta k \left(\frac{p_t}{R_g T_p} \right) (X_{CO})_{exit} \tag{7}$$

Since Ω and $(X_{CO})_{exit}$ are known, Equation (7) provides one relationship between η and k. An additional relationship is available through the relation between η and the Thiele modulus Φ, defined as

$$\Phi = R \left(\frac{\overline{S}_g \rho_a k}{D_e} \right)^{1/2} \tag{8}$$

However, the effective diffusivity must be known. Since knowledge of effective diffusivities at low porosity is inadequate, a value of D_e was estimated for the high porosity pellets and used with Equations (7) and (8) and the η versus Φ chart in (*15*) to evaluate k. Next, this value for k was assumed to be applicable for $\bar{\epsilon}_0 = 0.062$ and $\bar{\epsilon}_0 = 0.032$. Then η could be calculated directly from Equation (7), and Φ evaluated from the η versus Φ chart. Finally, Equation (8) was used to determine the effective diffusivity for the low and intermediate-porosity pellets.

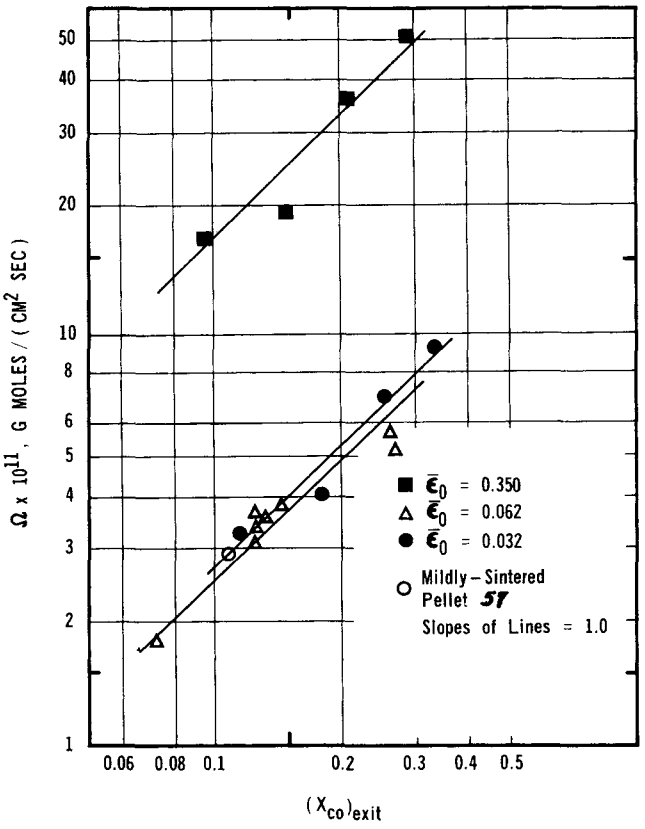

Fig. 5. Specific rates at 767°C. for different porosities.

Rate Constant *k*

Following the foregoing procedure, and employing the line for $\bar{\epsilon}_0 = 0.35$ in Figure 5 instead of the individual data points, the value of k at 767°C. was found to be 5.5×10^{-4} cm/s. The effective diffusivity used in this calculation was 0.0872 cm²/s. D_e was obtained by first evaluating a composite diffusivity D (which includes both Knudsen and bulk contributions) from the equation

$$\frac{1}{D} = \frac{1}{D_{k,CO}} + \frac{1}{D_{CO_2\text{-}CO}} \tag{9}$$

This expression is applicable for the equimolal counter diffusion of carbon dioxide and carbon monoxide existing in our system. The pore diameter used to evaluate $D_{k,CO}$ was 0.521×10^{-4} cm, as given in Table 1. The resultant value of D was 0.715 cm²/s. To convert D to an effective value for the porous nickel oxide pellet, the random-pore equation was used. For a monodisperse pore system the expression is

$$D_e = D(\bar{\epsilon}_0)^2 \tag{10}$$

This approach is equivalent to assuming a tortuosity factor given by

$$\alpha = \frac{D\bar{\epsilon}_0}{D_e} = \frac{1}{\bar{\epsilon}_0} = 2.86 \tag{11}$$

Such a value for α is within the range, $2 < \alpha < 6$, suggested by Satterfield (*15*) for unsintered materials.

Effective Diffusivities

Using the described procedure and $k = 5.5 \times 10^{-4}$ cm/s, effective diffusivities were calculated for the lower porosity pellets. The results are given in Table 2. Since hemispherical pellets were used for the runs at the lowest porosity, the spherical pellet form of the Thiele modules could not be used. Setterfield (*15*) proposed that the same Φ versus η chart could be employed for nonspherical geometry if R in Equation (8) is defined as

$$(R)_{hemi.} = 3 \frac{V}{S_{ex}} \tag{12}$$

This procedure was used. When η is low, which corresponds to our case, the effect of geometry on the η vs Φ relation becomes small.

With D_e available, the tortuosity factor can be calculated from Equation (11) for the intermediate and lowest porosity pellets. Results are given in Table 2. Other published values for porosities of a few percent could not be found. Reference has been made (*15*) to tortuosity factors of infinity for pellets, prepared from silver-calcium powders, with porosities of 0.04 and 0.1. For pellets of the same material at porosities of 0.3 to 0.6, α has decreased to the 6-10 level. The random-pore model predicts tortuosities from Equation (11) of 16 and 30 versus the experimental values of 92 and 176 for our nickel oxide pellets. A pore-model theory is needed for predicting effective diffusivities in slightly porous materials. Careful experimental measurements of porosities and diffusivities in such materials are also necessary. The indirect method of using reaction data to evaluate D_e, as illustrated in the work reported here, is not an accurate procedure.

Table 2 also shows effectiveness factors for the three porosity levels. The results for $\bar{\epsilon}_0 = 0.35$ are most reliable, since the Ω values are most accurate. At $\epsilon_0 = 0.35$, $\eta = 0.26$, suggesting that neither the shrinking-core model nor a zero-diffusion-resistance concept is applicable. At lower

porosities, the effectiveness factor decreases sharply. Even then the shrinking-core model is not approached since the effective reaction area is still much greater than the external surface. For example, for $\bar{\epsilon}_0 = 0.032$, the effective area $M_0 S_g \eta$ is about 180 cm², while S_{ex} is of the order of 6 cm².

Activation Energy

The effect of temperature upon the initial rate of reaction was measured using pellets of the lowest porosity level. The pellet properties and rate data are given in the lower sections of Tables 1 and 2. The rate constant was evaluated by employing Equation (7). Experimental values of Ω and $(X_{CO})_{exit}$ were known. The tortuosity factor of 176, determined from the data at 767°C., was employed to evaluate D_e from Equation (11). This value of D_e was used in Equation (8) which with the η versus Φ chart and Equation (7) could be solved for k and η. The resulting values of k are given in Table 2 and plotted versus $1/T$ in Figure 6.

The activation energy for the region 566 to 682°C., from the line in Figure 6, is 46.8 kcal./g.-mole. Comparison with literature data for this and similar systems is restricted because surface areas have not been measured. The data reported in the literature are based upon external areas and hence include diffusional effects. For example, an apparent activation energy E_A (for NiO reduction with CO) of 22.4 kcal./g.-mole has been reported by Vorontsov and Suikovskaya (*17*). The comparable value from our work obtained by plotting $(-dn/d\tau)_0/S_{ex}(X_{CO})_{exit}$ is 26.7 kcal./g.-mole. A decrease from 46.8 to 26.7 kcal./g.-mole between the true activation energy and E_A is, approximately, what would be expected (*15*) when the diffusion resistance is large.

For the reduction of NiO with H_2, in the temperature range 283 to 352°C., $E_A = 26.6$ kcal./g.-mole has been found (*12*). These authors also reported zero energy of activation in the region 600 to 1000°C., similar to the flat section above 682°C. observed in our work (Figure 6). The same effect has been noted for Fe_2O_3 reduction (*16*). An apparent energy of activation of 10-14 kcal./g.-mole was reported for the reduction of Fe_2O_3 with CO at 800 to 900°C. (*10*).

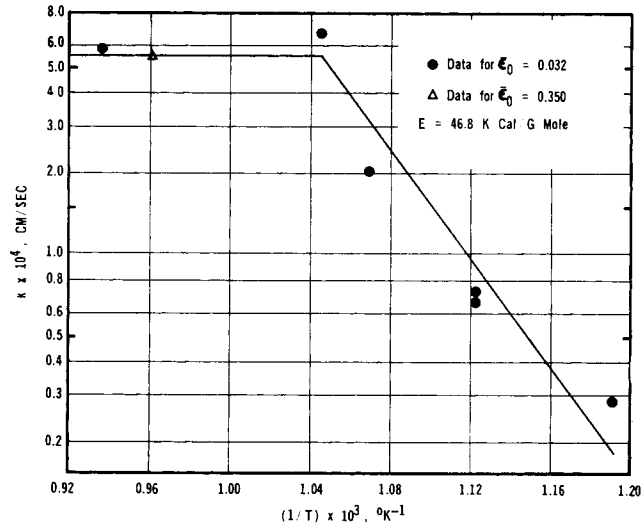

Fig. 6. Intrinsic kinetic constant versus temperature.

DISCUSSION

The induction period, noted in Figure 3 for the highest-porosity pellet, and the zero activation-energy region (Figure 6) provide some clues to the mechanism of the reduction process. The induction interval decreased as the carbon monoxide concentration increased, in agreement

Table 2. Rate Data

Pellet no.	$(X_{CO})_{exit}$	$\bar{\epsilon}_0$	t_p, °C.	$(-dn/d\tau)_0 \times 10^7$ g-moles/s	$\Omega \times 10^{11}$ g.-mole/s cm²	$\bar{D}_e \times 10^2$ cm²/s	$k \times 10^4$ cm/s	$\bar{\eta}$	$\bar{\alpha}$
19	0.125		767	7.00	3.45				
10	0.124		767	6.26	3.13				
16	0.131		767	7.00	3.52				
20	0.125		767	7.15	3.67				
8	0.193	0.062	767	7.15	3.81	0.048	(5.5)	0.036	92
27	0.072		767	3.36	1.80				
24	0.258		767	11.4	5.73				
12	0.267		767	10.3	5.21				
67	0.116		767	1.07	3.30				
36	0.338		767	3.97	9.18				
40	0.256	0.032	767	3.28	7.01	0.013	(5.5)	0.041	176
57	0.108		767	1.23	2.99				
33	0.180		767	2.25	4.03				
45	0.096		767	99.9	16.8				
74	0.210	0.35	767	246.0	36.5	8.72	5.5	0.26	2.86
28	0.148		767	104.0	19.3				
22	0.290		767	350.0	50.7				
90	0.249		682	2.40	6.07				
80	0.106		682	1.38	3.03				
60	0.080		682	1.03	3.25	0.012	6.8	0.039	
65	0.080		682	1.13	3.55				
54	0.080	0.032	617	0.271	0.974	0.011	0.74	0.12	(176)
49	0.080		617	0.236	0.916	0.011	0.66	0.12	
46	0.080		566	0.175	0.583	0.011	0.28	0.18	
59	0.080		662	0.438	1.61	0.012	2.0	0.076	
82	0.080		796	0.722	2.34	0.014	5.9	0.043	

with other studies (*2, 12, 16*). No induction time was apparent for the more severely sintered, lower-porosity pellets. These observations are in agreement with the concept (*2*) that before significant reaction can occur, nuclei of nickel atoms must be produced. According to this concept, reduction occurs by adsorption of carbon monoxide on the nickel nuclei, followed by migration to adjacent nickel oxide where oxygen is extracted from the nickel oxide lattice. The high activation energy suggests that the extraction step is slow. An alternate view is that carbon monoxide is chemisorbed directly on the nickel oxide, followed by extraction of oxygen. However, it is difficult to explain the induction period with this hypothesis.

The adsorption of carbon monoxide on nickel is known (*6, 8*) to occur rapidly while carbon monoxide adsorption on nickel oxide is hindered when carbon dioxide is also present (*14*), as in our experiments. Approximate extrapolation of low-temperature rates (*6*) indicate that carbon monoxide adsorption on nickel oxide would be three orders of magnitude less than the observed reduction rates for nickel oxide.

Nowak (*9*), in studies on the reduction of nickel oxide with hydrogen, using a NiO-on-Al_2O_3 catalyst, found evidence in support of the adsorption-migration theory. It was observed that adding small amounts of platinum increased the rate of reduction. Adding gold and silver did not enhance the rate. Since platinum readily adsorbs hydrogen, while gold and silver do not, adsorption of hydrogen on the platinum sites followed by migration to the adjacent nickel-oxide phase could explain the results.

The plateau in the Arrhenius plot (Figure 6) could be due to the effect of sintering at the freshly formed nickel-nickel oxide interphase. The Tamman temperature for nickel is 643°C. (*5*), which corresponds approximately to the temperature (682°C.) at which the activation energy approaches zero. At the Tamman temperature the sintering process is believed to involve an adhesion step during which individual particles are welded together. If this occurred at the nickel-nickel oxide interface, a decrease in interphase area would occur and cause a decrease in the rate. Such a suggestion has been made for the NiO-H_2 reduction reaction, and Charcosset (*2*) found a maximum in the rate of reduction at 350°C. Corresponding surface area measurements (B.E.T. method) indicated an increase in sintering at this temperature. Roman and Delmon (*13*) reported for the same system that the intrinsic energy of activation did not change, but that the apparent reduction in E was indeed due to a decrease in the nickel-nickel oxide interphase area.

While the evidence is not conclusive, it does favor an adsorption (on Ni nuclei)—migration mechanism rather than adsorption of carbon monoxide on nickel oxide.

ACKNOWLEDGMENT

Partial support of the Petroleum Research Fund, American Chemical Society, Grant 4155 is gratefully acknowledged.

NOTATION

D = composite diffusivity of CO in CO_2; D_k refers to the Knudsen diffusivity, $D_{CO_2\text{-}CO}$ to the bulk diffusivity, and D_e to the effective diffusivity in the pores of the NiO pellet, cm^2/s

$D(\delta)$ = pore volume distribution function, $dV_\delta/d\delta$, cm^2.

E = intrinsic activation energy; E_A indicates the apparent activation energy, kcal./mole

F = flow rate of feed ($CO + CO_2$) to reactor, g.-mole/s

k = intrinsic rate constant, cm/s

L_i = length of pore of diameter δ_i, cm.

M_0 = initial weight of NiO pellet, g.

ΔM = increase of weight of pellet, g.

n = moles of NiO, g.-mole

$-\left(\frac{dn}{d\tau}\right)_0$ = initial rate of reaction per pellet, g.-mole/s

p_t = total pressure, atm.

R = pellet radius; $(R)_{\text{hemi.}}$ = equivalent radius of hemispherical pellet, cm

R_g = gas constant

S_{ex} = external area of pellet, cm^2

S_g = surface area of pellet, cm^2/g

t = temperature, °C. (T = °K.); t_g = temperature measured by thermocouple in gas phase; t_p = pellet temperature

V = volume of pellet, cm^3

V_δ = volume of pores

X_{CO} = mole fraction CO in gas

Greek Letters

α = tortuosity factor

δ = pore diameter, cm.

ϵ = porosity; ϵ_T = total porosity of the pellet; ϵ_s = porosity of closed pores; ϵ_0 = porosity of open pores

Ω = rate of reaction per unit surface area, g.-mole/(sec.)(sq. cm.)

ρ = density; ρ_a = apparent density of the pellet; ρ_s = composite density of solid phase plus closed pores, g./cu. cm.

η = effectiveness factor at initial conditions

Φ = Thiele modules

τ = time, sec.

— = denotes average value

0 = denotes initial ($\tau = 0$) value

LITERATURE CITED

1. Coulson, J. M., and J. F. Richardson, "Chemical Engineering," Pergamon Press, London, England (1954).
2. Charcosset, H., R. Frety, Y. Trambouze, M. Prettre, in "Reactivity of Solids," J. Mitchell (ed.), Wiley, N. Y. (1969).
3. Costa, E. C., and J. M. Smith *AIChE J.*, **17**, 947 (1971).
4. Frety, R., *Ann. Chim.*, **4**, 453 (1969).
5. Habashi, F., "Principles of Extractive Metallurgy," Gordon and Breach, N. Y. (1969).
6. Hayward, D. O., and B. M. Trapnell, "Chemisorption," Butterworths, London, England (1964).
7. Kolthoff, I. M., and E. B. Sandell, "Textbook of Quantitative Inorganic Analysis," Macmillan, N. Y. (1952).
8. Lapoujalade, J., *J. Chimie Physique*, **67**, 74 (1970).
9. Nowak, J., *J. Phys. Chem.*, **73**, 3790 (1969).
10. Osman, M. A., F. S. Manning, W. O. Philbrook, *AIChE J.*, **12**, 685 (1966).
11. Pratt, N. H., *Trans. Inst. Chem. Engrs.*, **25**, 163 (1947).
12. Rozhdestvenskii, V. P., L. M. Volgina, and T. P. Strokova, *Zh. Pr. Khim.*, **40**, 705 (1967).
13. Roman, A., and B. Delmon, C. R. Acad. Sc. Paris *271, B*, 77 (1970).
14. Ranc, R. E., and S. J. Teichner, *Bull. Soc. Chim. France*, **5**, 1717 (1967).
15. Satterfield, C. N., "Mass Transfer in Heterogeneous Catalysis," MIT Press, Cambridge (1970).
16. Themelis, N. J., and W. H. Gauvin, Can. Min. Met. Bull. 444 (1962).
17. Vorontsov, E. S., V. D. Suikovskaya, *Izv. Vissh. Ucheb. Zaved. Chern. Met.*, **12**, 5 (1969).
18. Watanabe, M., *Bull. Inst. Phys. Chem. Research*, Tokyo, **9**, 477 (1930).
19. Yagi, S., D. Kunii, *Chem. Eng. Sci.*, **16**, 364, 372, 380 (1961).

Manuscript received November 1, 1971; revision received December 16, 1971; paper accepted December 16, 1971.